Ginzburg-Landau Theory for a p-Wave Sr_2RuO_4 Superconductor: Vortex Core Structure and Extended London Theory

R. Heeb
Theoretische Physik, ETH Hönggerberg, CH-8093 Zürich, Switzerland

D.F. Agterberg
National High Magnetic Field Laboratory, Florida State University, Tallahassee, Florida, 32306, USA

(July 1998)

Abstract

Based on a two dimensional odd-parity superconducting order parameter for Sr_2RuO_4 with p-wave symmetry, we investigate the single vortex and vortex lattice structure of the mixed phase near H_{c1}. Ginzburg-Landau calculations for a single vortex show a fourfold structure with an orientation depending on the microscopic Fermi surface properties. The corresponding extended London theory is developed to determine the vortex lattice structure and we find near H_{c1} a centered rectangular vortex lattice. As the field is increased from H_{c1} this lattice continuously deforms until a square vortex lattice is achieved. In the centered rectangular phase the field distribution, as measurable through μSR experiments, exhibits a characteristic two peak structure (similar to that predicted in high temperature and borocarbide superconductors).

I. INTRODUCTION

With the observation of zero resistivity in Sr_2RuO_4 below $T_c = 0.93$K, Maeno *et al.*[1] discovered the first layered perovskite compound without CuO_2 planes showing superconductivity. Recent experimental and theoretical research provides considerable evidence that the superconducting state of Sr_2RuO_4 is of an odd-parity p-wave symmetry.

Classifying the superconducting states of a generalized BCS theory[2], the mean fields

$$\Delta_{s,s'}(\boldsymbol{k}) = -\sum_{\boldsymbol{k'},\sigma,\sigma'} V_{s's\sigma\sigma'}(\boldsymbol{k},\boldsymbol{k'})\langle c_{\boldsymbol{k'},\sigma} c_{-\boldsymbol{k'},\sigma'}\rangle \tag{1}$$

are split into singlet and triplet pairing states making use of the antisymmetry condition $\hat{\Delta}(\boldsymbol{k}) = -\hat{\Delta}^T(-\boldsymbol{k})$. While singlet states are described through an even scalar function $\psi(\boldsymbol{k})$ in the form $\hat{\Delta}(\boldsymbol{k}) = i\hat{\sigma}_y\psi(\boldsymbol{k})$, triplet states take the form

$$\hat{\Delta}(\boldsymbol{k}) \propto i(\boldsymbol{d}(\boldsymbol{k})\cdot\hat{\boldsymbol{\sigma}})\hat{\sigma}_y, \tag{2}$$

where $\boldsymbol{d}(\boldsymbol{k}) = -\boldsymbol{d}(-\boldsymbol{k})$ is an odd vector function[3]. Taking into account the crystal symmetry, the $\boldsymbol{k}$-dependent functions $\psi(\boldsymbol{k})$ and $\boldsymbol{d}(\boldsymbol{k})$ have to belong to an irreducible representation of the lattice point group, in our case the tetragonal point group D_{4h}.

Initial proposals of odd parity superconductivity in Sr_2RuO_4 were founded on the itinerant ferromagnetism of related ruthenate compounds and on the similarities between Sr_2RuO_4 and ^{3}He in the Fermi liquid corrections produced by electronic correlations[4]. Recently, muon spin rotation (μSR) measurements[5] have observed that a spontaneous magnetization begins to develop below T_c. This finding is most naturally explained in terms of a time reversal ($\mathcal{T}$) symmetry breaking state implying a multiple component representation of the D_{4h} point group. Furthermore, since the electronic structure of Sr_2RuO_4 is quasi-two dimensional, a gap function with a strong k_z-dependence is unlikely. Of the remaining two odd or even two-component representations of D_{4h}, the odd Γ_{5u}^- representation with basis functions $\{\boldsymbol{d}_1(\boldsymbol{k}), \boldsymbol{d}_2(\boldsymbol{k})\} = \{\hat{\boldsymbol{z}}k_x, \hat{\boldsymbol{z}}k_y\}$ is the only without nodes at $k_z = 0$ and therefore is most likely to be realized in Sr_2RuO_4.

In Ginzburg-Landau (GL) theory, we deal with order parameters $\eta_j(\boldsymbol{R})$ depending only on the center-of-mass coordinate $\boldsymbol{R}$, defined through

$$\hat{\Delta}(\boldsymbol{R},\boldsymbol{k}) = \sum_{j=1}^{2} \eta_j(\boldsymbol{R})\; i(\boldsymbol{d}_j(\boldsymbol{k})\cdot\hat{\boldsymbol{\sigma}})\hat{\sigma}_y. \tag{3}$$

As usual we switch the transformation behavior from the basis functions $\boldsymbol{d}_j(\boldsymbol{k})$ to the order parameter components η_j. The components (η_1,η_2) then share the rotation-inversion symmetry properties of (k_x,k_y), and the broken $\mathcal{T}$-state is $(\eta_1,\eta_2) \propto (1,\pm i)$. Based on this order parameter, one of us[6] examined the vortex lattice structures of Sr_2RuO_4 near H_{c2}: for an applied finite field H along a high symmetry direction in the basal ab-plane, two vortex lattice phases have been found with a second superconducting transition between them, while a square vortex lattice has minimal energy when the field is along the c-axis. Band structure calculations[7–9] reveal that the density of states near the Fermi surface is mainly due to the four Ru $4d$ electrons, which hybridize strongly with the O $2p$ orbitals and give rise to three bands crossing the Fermi surface, labeled α, β and γ (see Ref. 7).

Within the model of orbital dependent superconductivity[10], the orientation of the square lattice mentioned above depends on which of the Fermi surface sheets is responsible for the superconductivity. Recent experiments using SANS[11] show a square vortex lattice aligned with the crystal lattice in a wide range of the phase diagram, indicating that the γ sheet (due to the xy - Wannier functions) of the Fermi surface shows the superconducting transition[6]. Assuming that ferromagnetic spin fluctuations are responsible for the superconducting state, this finding is in agreement with ^{17}O NMR experiments[12] showing strong ferromagnetic spin enhancements only in the Ru $4d_{xy}$ orbitals.

In this paper we investigate the single vortex core structure and the geometry of the vortex lattice near the lower critical field H_{c1}. We start from the Ginzburg-Landau theory for the two-component order parameter (η_1, η_2) and solve numerically for the vortex core structure of an isolated vortex. Next, we derive an extended London model valid for fields near H_{c1} and large GL parameters κ and determine the geometric structure of the vortex lattice. We find hexagonal lattices near H_{c1}, deforming into square lattices upon increasing the applied field. Taking the γ sheet as relevant for superconductivity, the orientation of the square lattices is in agreement with experiments[11]. The individual vortex cores show square deformations. This vortex core structure is observable through scanning tunneling microscopy (STM) measurements since the in-plane coherence length of 900 Å is well within the spatial resolution required by STM. Alternatively, Bitter decoration studies near H_{c1} can be used to detect the predicted field dependent transition between hexagonal and square lattice, which would complete the picture found by SANS-measurements for higher applied fields[11]. A further characteristic of the hex-to-square transition is the peak splitting in the field distribution calculated in Sec. IV and measurable in μSR experiments. Note that a similar transition has been predicted in borocarbide[13,14] and high-T_c superconductors[15] and has been observed recently in the borocarbide materials[16].

II. GINZBURG-LANDAU RESULTS FOR THE VORTEX STRUCTURE

We start from the Ginzburg-Landau free-energy density (f) for the two-dimensional representation Γ^-_{5u} of the tetragonal point group, with the Ginzburg-Landau coefficients determined within a weak-coupling approximation in the clean limit. These two approximations seem reasonable for Sr_2RuO_4 given the ratios[17] $T_c/\epsilon_F \sim 10^{-4}$ and $l/\xi \approx 8$ (here T_c denotes the critical temperature, ϵ_F the Fermi energy, l the mean free path and ξ the coherence length). In usual dimensionless units, we have[18]

$$\begin{aligned} f = & -(|\eta_+|^2 + |\eta_-|^2) + \frac{1}{2}\left(|\eta_+|^4 + |\eta_-|^4\right) + 2\,|\eta_+|^2|\eta_-|^2 + \frac{\nu}{2}\left[(\eta_-\eta_+^*)^2 + (\eta_-^*\eta_+)^2\right] \\ & + B^2 + |\boldsymbol{D}\eta_+|^2 + |\boldsymbol{D}\eta_-|^2 \\ & + \frac{1+\nu}{2}\left[(D_x\eta_+)(D_x\eta_-)^* + (D_x\eta_-)(D_x\eta_+)^*\right] \\ & - \frac{1+\nu}{2}\left[(D_y\eta_+)(D_y\eta_-)^* + (D_y\eta_-)(D_y\eta_+)^*\right] \\ & + \frac{1-\nu}{2\,i}\left[(D_x\eta_+)(D_y\eta_-)^* + (D_y\eta_+)(D_x\eta_-)^*\right] \\ & - \frac{1-\nu}{2\,i}\left[(D_x\eta_+)^*(D_y\eta_-) + (D_y\eta_+)^*(D_x\eta_-)\right], \end{aligned} \tag{4}$$

where $\eta_\pm = (\eta_1 \pm i\eta_2)/\sqrt{2}$, $\boldsymbol{B} = \nabla \wedge \boldsymbol{A}$, $D_\mu = -i\,\nabla_\mu/\kappa - A_\mu$, f is in units $B_c^2/4\pi$, lengths are in units of the penetration depth λ, $\boldsymbol{B}$ is in units $\sqrt{2}B_c = \Phi_0/(2\pi\lambda\xi)$, $\alpha = \alpha_0(T - T_c)$, and $\kappa = \lambda/\xi$. The anisotropy $\nu = (\langle v_x^4\rangle - 3\langle v_x^2 v_y^2\rangle)/(\langle v_x^4\rangle + \langle v_x^2 v_y^2\rangle)$ is a parameter that measures the tetragonal distortion of the Fermi surface ($\langle\cdot\rangle$ denotes averaging over the Fermi surface; note $|\nu| \leq 1$ and $\nu = 0$ for a cylindrical geometry). The free energy f is invariant under a simultaneous rotation of 45° around the c-axis and changing sign of ν. This implies that all results derived below for $\nu < 0$ can be transformed into the corresponding results for positive $\nu > 0$ by a simple rotation, and we limit ourselves to the case $\nu < 0$. Further we deal only with external fields applied along the c-axis allowing us to omit all terms containing z-derivatives.

At zero applied field the two degenerate solutions $(\eta_+, \eta_-) = (1, 0)$ and $(\eta_+, \eta_-) = (0, 1)$ minimize the free energy f. For nonzero applied field, the degeneracy is lifted, and depending on the direction of the applied field only one component $\eta_\pm$ is stable. Throughout this paper we will fix the dominant order parameter to be η_-. The asymptotic vorticity of the dominant η_--component then determines the field direction along the positive or negative z-axis. In the spatially inhomogeneous situations considered below, the second component η_+ is driven through the mixed gradient terms [gradient terms such as $(D_x\eta_+)^*(D_y\eta_-)$] and decays far away from the defect. Note, that to each solution $\{\eta_-, \eta_+, \boldsymbol{B}\}$ a symmetric counterpart with reversed field direction exists

$$\{\eta_-, \eta_+, \boldsymbol{B}\} \quad \rightarrow \quad \{\eta_+^*, \eta_-^*, -\boldsymbol{B}\}. \tag{5}$$

Below, we first examine the asymptotic solutions of the GL-equations for $\nu = 0$. Second, we use the $\nu = 0$-solution and carry out perturbation theory in ν to obtain the asymptotic solutions for $\nu \neq 0$ (we ignore the coupling to the vector potential in the latter case).

In the cylindrical case ($\nu = 0$) the problem exhibits rotational symmetry. Restricting to fields $\boldsymbol{B} = B(r)\boldsymbol{e_z}$, the solution has the structure

$$\begin{aligned} \eta_-(\boldsymbol{r}) &= e^{in\theta}\eta_-(r), \\ \eta_+(\boldsymbol{r}) &= e^{i(n+2)\theta}\eta_+(r), \\ \boldsymbol{A}(\boldsymbol{r}) &= A(r)\boldsymbol{e_\theta}, \end{aligned} \tag{6}$$

where (r, θ) are polar coordinates and n denotes the phase winding of the topological defect driving the vortex in the main superconducting component. The relative phase $e^{i2\theta}$ between η_- and η_+ corresponds to an angular momentum difference $\Delta l = 2$ and comes in through the specific form $(D_x + iD_y)^2$ of the mixed gradient terms for $\nu = 0$. The solutions for $n = \pm 1$ are the most stable ones. The small r expansion to cubic order takes the form

$$\begin{aligned} n = 1: \qquad \eta_-(\boldsymbol{r}) &\sim \left(m_1^0 r - \left(\frac{3}{2}p_3^0 + \frac{\kappa^2}{8}m_1^0\left(1 + \frac{2}{\kappa}a_1^0\right)\right)r^3\right)e^{i\theta}, \\ \eta_+(\boldsymbol{r}) &\sim p_3^0 r^3\, e^{3i\theta}, \\ A(r) &\sim a_1^0 r - \frac{(m_1^0)^2}{8\kappa}\, r^3, \\ n = -1: \qquad \eta_-(\boldsymbol{r}) &\sim \left(m_1^0 r + \frac{\kappa^2}{6}\left(\frac{1}{2}p_1^0 - m_1^0 + \frac{3}{\kappa}a_1^0\left(m_1^0 + p_1^0\right)\right)r^3\right)e^{-i\theta}, \end{aligned} \tag{7}$$

$$\eta_+(\boldsymbol{r}) \sim \left(p_1^0 r + \frac{\kappa^2}{6} \left(\frac{1}{2} m_1^0 - p_1^0 - \frac{3}{\kappa} a_1^0 \left(m_1^0 + p_1^0 \right) \right) r^3 \right) e^{i\theta},$$
$$A(r) \sim a_1^0 r - \frac{(p_1^0)^2 - (m_1^0)^2}{8\kappa} r^3, \tag{8}$$

where m_1^0, $p_{1,3}^0$, and a_1^0 are the first expansion coefficients of η_-, η_+, and A, to be determined by matching this small r expansion to the asymptotics at $r \to \infty$. The latter reads

$$\eta_-(\boldsymbol{r}) = (1 - m(r))\, e^{in\theta},$$
$$\eta_+(\boldsymbol{r}) = p(r)\, e^{i(n+2)\theta},$$
$$A(r) = \pm \frac{1}{\kappa r} + a(r), \tag{9}$$

where the $\pm$ stands for $n = \pm 1$. The asymptotic form of the GL-equations requires the three functions $m(r)$, $p(r)$, and $a(r)$ to be of the form

$$\eta_-(\boldsymbol{r}) \sim \left(1 - \frac{(n+2)^2}{2\kappa^2 r^2} \right) e^{in\theta},$$
$$\eta_+(\boldsymbol{r}) \sim \frac{n^2 + 2n}{2\kappa^2 r^2}\, e^{i(n+2)\theta}, \tag{10}$$

if we ignore the vector potential $A(r) = 0$. For the general case ($A(r) \neq 0$) the main asymptotics is an exponential decay

$$a(r), m(r), p(r) \sim e^{-r/\Lambda}, \tag{11}$$

which is a consequence of transverse screening. From Fig. 1 we see, that for reasonably large κ this exponent Λ approaches 1, which equals the usual penetration depth in dimensionless units.

We proceed now with the anisotropic case $\nu \neq 0$ (here we neglect the vector potential). An expansion to first order in ν produces the following result for small r

$$n = 1: \qquad \eta_-(\boldsymbol{r}) \sim \left(m_1^0 r - \frac{\kappa^2 m_1^0 + 12 p_3^0}{8} r^3 \right) e^{i\theta} + \nu \left(\frac{\kappa^2 m_1^0 + 12 p_3^0}{16} - \frac{3 g_{-,3}^0}{2} \right) r^3 e^{-i\theta},$$
$$\eta_+(\boldsymbol{r}) \sim p_3^0 r^3\, e^{3i\theta} + \nu g_{-,3}^0 r^3\, e^{-i\theta}, \tag{12}$$
$$n = -1: \qquad \eta_-(\boldsymbol{r}) \sim \left(m_1^0 r + \frac{\kappa^2}{12} (p_1^0 - 2m_1^0) r^3 \right) e^{-i\theta} + \nu g_{+,3}^0 r^3\, e^{3i\theta},$$
$$\eta_+(\boldsymbol{r}) \sim \left(p_1^0 r + \frac{\kappa^2}{12} (m_1^0 - 2p_1^0) r^3 \right) e^{i\theta} + \nu f_{-,3}^0 r^3\, e^{-3i\theta}, \tag{13}$$

and for large r

$$\eta_-(\boldsymbol{r}) \sim \left(1 - \frac{(n+2)^2}{2\kappa^2 r^2} \right) e^{in\theta} - \nu \frac{n}{2\kappa^2 r^2} \left(e^{i(n+4)\theta} + 3 e^{i(n-4)\theta} \right),$$
$$\eta_+(\boldsymbol{r}) \sim \frac{n^2 + 2n}{2\kappa^2 r^2}\, e^{i(n+2)\theta} + \nu \frac{n}{\kappa^2 r^2} \left(e^{i(n+6)\theta} + e^{i(n-2)\theta} \right). \tag{14}$$

The additional coefficients $g^0_{\pm,3}$ and $f^0_{\pm,3}$ are the first expansion coefficients of the higher angular momentum states ($f^0_{\pm,3}$ from $\eta_+ \sim e^{i(n+2\pm4)\theta}$ and $f^0_{\pm,3}$ from $\eta_- \sim e^{i(n\pm4)\theta}$), which arise for $\nu \neq 0$. Comparing the condensation energy for the two cases $n = \pm 1$ we find that the $(n = -1)$-case is the more stable: the admixed η_+ order parameter rises linearly in the center rather than cubic as is the case for $n = 1$, and the asymptotic phase turns of η_+ are the same in the center and for large r (which is also an argument against off-centered zeroes as seen for example in $d_{x^2-y^2}$-superconductors). Both points lead to a higher gain in condensation energy, which should stabilize the $(n = -1)$-solution. Our numerical Ginzburg-Landau results (described in the next paragraph) for the critical fields $H_{c1} = \epsilon_l \kappa/4\pi$ confirm this finding: for $\kappa = 2.5$ and $\nu = -0.3$, we obtain

$$H_{c1}(n = -1) = 0.43 B_c,$$
$$H_{c1}(n = 1) = 0.47 B_c,$$

demonstrating the stability of the $(n = -1)$-solution compared to $(n = 1)$. The corresponding s-wave result is $H_{c1} = 0.48 B_c$.

To obtain complete numerical solutions, we minimize the free energy density on a two-dimensional grid. The minimization is carried out by relaxing an initial configuration $\eta_+ = 0$, $\eta_- = \tanh(r)\, e^{\pm i\theta}$ and $\boldsymbol{A} = 0$ iteratively. Indeed we find that the energetically favorable $(n = -1)$-solution shows no off-centered zeroes in η_+. A contour plot of the absolute value of the dominant η_- (a) and η_+-component (b) is displayed in Fig. 2. The admixed η_+ solution shows a fourfold structure with a maximal amplitude along the axes. In addition the vortex core center of the dominant order parameter is distorted with marked elongations along the diagonals of the crystal lattice for $\nu < 0$ (and analogously along the axes for $\nu > 0$). This behavior is understood recalling the properties of the Fermi surface. For $\nu < 0$, the density of states (DOS) at the Fermi surface is larger along the axes than along the diagonals. A larger DOS however implies also a larger effective mass, which reduces the coherence length and thus the size of the vortex. Finally, the distribution of the absolute value of the B_z-field (see Fig. 3) also shows clear square deformations aligned with the underlying crystal lattice.

On the other hand, in the unstable $(n = 1)$-case the admixed component η_+ exhibits a negative phase turn around the center, and consequently four off-centered zeroes with positive phase turn are needed to match up this phase $e^{-i\theta}$ at small r to the asymptotic phase $e^{3i\theta}$ at large r. This pattern is qualitatively well known from analog GL-calculations for s-admixture in $d_{x^2-y^2}$ high-T_c superconductors[19–23]. The dominant component η_- and the B_z-field show similar features as in the stable case discussed above.

III. EXTENDED LONDON THEORY

We wish to determine the form of the vortex lattice close to H_{c1}. Instead of solving the Ginzburg-Landau free energy directly, here we follow an idea recently developed in the context of $d_{x^2-y^2}$-wave superconductors with a weak admixing of an s-component[15]. We first integrate out the admixed component, leading to a one-component free energy density. We assume $\kappa \gg 1$ and $\nu \ll 1$ and use London approximation to obtain an effective free energy density which depends only on the field B and which can be minimized with respect to the geometry of the vortex lattice. Though our results will be quantitatively inaccurate for the low-κ Sr_2RuO_4 material, we still expect to obtain a qualitatively correct picture.

The Ginzburg-Landau equation for η_+ to first order in $|\eta_+|/|\eta_-|$ reads

$$0 = -\eta_+ + 2\,|\eta_-|^2\eta_+ + \boldsymbol{D}^2\,\eta_+ + \frac{1+\nu}{2}\,(D_x^2 - D_y^2)\,\eta_- - \frac{1-\nu}{2\,i}\,(D_xD_y + D_yD_x)\,\eta_-. \qquad (15)$$

Within London theory the dominant component η_- has modulus unity (see Eq. (18)) and the first three terms lead to the expression $(1+\boldsymbol{D}^2)\,\eta_+$. Solving formally for η_+ and substituting this expression into the free energy density, we obtain the effective one-component Ginzburg-Landau free energy

$$f = -|\eta_-|^2 + \frac{1}{2}\,|\eta_-|^4 + |\boldsymbol{D}\eta_-|^2 - \eta_-^*\,\mathcal{P}(\boldsymbol{D},\nu)\left(1+\boldsymbol{D}^2\right)^{-1}\mathcal{P}(\boldsymbol{D},\nu)\,\eta_- + B^2, \qquad (16)$$

with

$$\mathcal{P}(\boldsymbol{D},\nu) = \frac{1+\nu}{2}\,(D_x^2 - D_y^2) - \frac{1-\nu}{2\,i}\,(D_xD_y + D_yD_x). \qquad (17)$$

Here we have consistently neglected all terms of order η_+^4, $\nu\eta_+^2$, and higher.

Following the usual scheme for London approximation we replace the order parameter η_- and its derivative by the superfluid velocity $\boldsymbol{v}$

$$\begin{aligned}\eta_- &= e^{i\phi(\boldsymbol{x})},\\ \boldsymbol{D}\eta_- &= (\frac{1}{\kappa}\,\boldsymbol{\nabla}\phi(\boldsymbol{x}) - \boldsymbol{A})\,e^{i\phi(\boldsymbol{x})} \equiv \frac{1}{\kappa}\,\boldsymbol{v}\,e^{i\phi(\boldsymbol{x})}.\end{aligned} \qquad (18)$$

Keeping only terms up to second order in $\boldsymbol{v}$ and up to first order in the anisotropy parameter ν, we obtain the London free energy in Fourier representation

$$\begin{aligned}f(\boldsymbol{k}) = &-\frac{1}{2} + \frac{1}{\kappa^2}\,\boldsymbol{v}^2 + B^2\\ &-\frac{1}{4\kappa^4}\,\frac{1}{1+k^2/\kappa^2}\left(k^2\boldsymbol{v}^2 + 2\nu\left[(k_x^2-k_y^2)\,(v_x^2-v_y^2) - (2\,k_xk_y)\,(2\,v_xv_y)\right]\right).\end{aligned} \qquad (19)$$

Here, all quadratic expressions in $\boldsymbol{v}$ and B have to be understood as $v_iv_j = v_i(\boldsymbol{k})v_j(-\boldsymbol{k})$ (the results for vorticity $n=\pm1$ are the same on this level of calculation; they would differ if one included higher orders in $\boldsymbol{v}$).

Next, we eliminate $\boldsymbol{v}$. We obtain an equation connecting B and $\boldsymbol{v}$ by variation of the London free energy Eq. (19) with respect to the vector potential $\boldsymbol{A}$. The corresponding Euler-Lagrange equation reads

$$i\,\kappa^3\,\boldsymbol{k}\wedge\boldsymbol{B} = \kappa^2\,\boldsymbol{v} - \frac{1}{4}\,\frac{1}{1+k^2/\kappa^2}\left(k^2\boldsymbol{v} + 2\nu\left[(k_x^2-k_y^2)\,(v_x\hat{\boldsymbol{x}} - v_y\hat{\boldsymbol{y}}) - (2\,k_xk_y)\,(v_x\hat{\boldsymbol{y}} + v_y\hat{\boldsymbol{x}})\right]\right). \qquad (20)$$

We solve this equation for $\boldsymbol{v}$ up to first order in ν and substitute the solution back into the London free energy density (Eq. (19)), to obtain

$$\begin{aligned}f(\boldsymbol{q}) &= -\frac{1}{2} + \left[1 + q^2\kappa^2\frac{1+q^2}{(1+\frac{3}{4}\,q^2)^2}\left(1 + \frac{3}{4}\,q^2 - \frac{\nu}{2}\Big(\frac{(q_x^2-q_y^2)^2}{q^2} - \frac{(2\,q_xq_y)^2}{q^2}\Big)\right)\right]B^2\\ &\equiv -\frac{1}{2} + J(\boldsymbol{q},\nu,\kappa)\,B^2,\end{aligned} \qquad (21)$$

where we introduced the short notation

$$\boldsymbol{q} = \frac{1}{\kappa}\,\boldsymbol{k}. \tag{22}$$

The variation with respect to $B(\boldsymbol{k})$ leads to the extended London equation $J(\boldsymbol{q},\nu,\kappa)B(\boldsymbol{k}) = 0$ (in the limit $\kappa \to \infty$ we recover the well-known result $(1+k^2)B(\boldsymbol{k}) = 0$ (no sources)).

IV. VORTEX LATTICE CLOSE TO H_{c1}

We generate the vortex lattice by introducing the corresponding source terms at the vortex core positions into the London equations. A convenient form for these source terms is[24]

$$\sigma(\boldsymbol{r}) = \kappa \sum_j e^{-\kappa^2(\boldsymbol{r}-\boldsymbol{r}_j)^2/2}, \tag{23}$$

where the sum leads over all positions $\boldsymbol{r}_j$ of the vortex lattice. The magnetic field and the Gibbs free energy for the vortex lattice read

$$\begin{aligned} B(\boldsymbol{r}) &= \overline{B} \sum_{\boldsymbol{q}_j} \frac{e^{i\kappa \boldsymbol{q_j} \boldsymbol{r}}\, e^{-q_j^2/2}}{J(\boldsymbol{q}_j,\nu,\kappa)} \\ \mathcal{G}(H) &= \overline{B}^2 \sum_{\boldsymbol{q}_j} \frac{e^{-q_j^2}}{J(\boldsymbol{q}_j,\nu,\kappa)} - 2H\overline{B}, \end{aligned} \tag{24}$$

where the specific form of the vortex lattice is given by the reciprocal lattice vectors $\boldsymbol{q}_j$. We parameterize the unit cell in real space through the angles θ_1 and θ_2, the ratio of the lengths of the unit vectors ζ and the average field $\overline{B}$ (see Fig. 4), where the first three parameters describe the geometry and $\overline{B}$ the size of the cell. The lattice geometry depends on the applied field H and is determined by minimizing the Gibbs free energy $\mathcal{G}(H)$ given in Eq. (24) with respect to the unit cell parameters. Writing the operator $J(\boldsymbol{q},\nu,\kappa)$ in the form

$$J(\boldsymbol{q},\nu,\kappa) = 1 + \kappa^2 \frac{1+q^2}{(1+\frac{3}{4}\,q^2)^2} \left(q^2 + \frac{3}{4}\,q^4 - \frac{\nu}{2}\,q^4 \cos 4\phi_{\boldsymbol{q}} \right), \tag{25}$$

it is obvious that a change of sign in ν still corresponds to a rotation in real and reciprocal space by 45°. We thus restrict the discussion again to negative values of ν. The resulting vortex lattices exhibit a centered rectangular unit cell with the main axes aligned along the diagonals of the underlying crystal. Without loss of generality we thus assume $\theta_1 = \pi/4 - \theta_2/2$ and $\zeta = 1$ in the remainder of the paper. In Fig. 5 we plot the angle θ_2 minimizing the Gibbs free energy for different values of ν versus the field H (Fig. 5a: $\kappa = 25.0$, Fig. 5b: $\kappa = 5.0$). For large enough values of the anisotropy parameter ν, the vortex lattice evolves from hexagonal at low applied fields to square at high fields. The lattices found in our calculations ($\nu < 0$) are always aligned with the underlying lattice (see Fig. 6). For decreasing κ, the crossover to a square lattice approaches to the lower critical field H_{c1} and occurs at lower anisotropies ν, an effect which is believed to be even stronger if one

would include all nonlinearities into the theory. These results are in good agreement with recent experimental data of Riseman et al.[11], who find an aligned square lattice in Sr_2RuO_4 down to very small fields in the phase diagram.

Apart form the vortex lattice symmetry, the shape of the individual vortices as well as the corresponding field distributions is of interest. The former, because STM-measurements are able to determine the form of the individual vortices directly, and the latter since the field distribution is the typical result of μSR-measurements. While the shape of the B-field around the vortex core is perfectly circular for $\nu = 0$ over the whole range of the applied field H, we find square deformations of the B-field for negative values of ν (see Fig.6). This is in agreement with the single vortex results obtained in the previous section, which also exhibits the corresponding deformation of the fields around the vortex core.

Experiments using μSR can observe the field distribution

$$P(B) = \frac{1}{V_{\rm uc}} \int_{V_{\rm uc}} d^2\boldsymbol{r}\, \delta\left(B - B(\boldsymbol{r})\right). \tag{26}$$

In Fig. 7, characteristic results are shown for two cases $\kappa = 25.0, H = 3.1$ (a) and $\kappa = 5.0, H = 0.5$ (b). While at $\nu = 0$ the field distribution shows only one peak with a small shoulder towards the minimal field value, the situation for $\nu \neq 0$ is quite different. With increasing $|\nu|$ the $\nu = 0$-peak splits into two due to the appearance of two nonequivalent classes of saddle points in the B-field. Upon further increase of $|\nu|$, the low field peak gradually vanishes and finally develops into a broad shoulder.

V. CONCLUSIONS

We have investigated the single vortex and vortex lattice structure of Sr_2RuO_4 near H_{c1}, assuming a weak-coupling, clean limit description of the 2D odd-parity Γ_{5u}^- symmetry of the superconducting state in Sr_2RuO_4. The stable single vortex solution (denoted $(1,-1)$) takes the asymptotic form $(\eta_+, \eta_-) = (p(r)e^{i\theta}, [1-m(r)]e^{-i\theta})$. A second low energy vortex solution has the asymptotic form $(\eta_+, \eta_-) = (p(r)e^{3i\theta}, [1-m(r)]e^{i\theta})$ (denoted $(3,1)$). Solutions of the latter type appear to be the minimal ones for d-wave superconductors with an admixed s-wave component. Here, the symmetry allows for the competing $(1,-1)$-solution which has a lower energy as it contains fewer nodes and decays slower near the vortex core. The stable $(1,-1)$-solution shows clear four-fold deformations due to the anisotropy of the density of states at the Fermi surface. Current experimental results on the vortex lattice structure point towards an elongation of the vortex along the crystal lattice diagonals, in agreement with our theoretical analysis. A direct proof of such a structure should be observable through STM measurements.

The structure of the vortex lattice has been determined using an extended London approach where the admixed η_+ component has been integrated out. The resulting London theory predicts that with increasing field the vortex lattice will continuously deform from a hexagonal to a square lattice. The orientation of the square vortex lattice depends on the anisotropy parameter ν: For $\nu < 0$ the square vortex lattice is aligned with the crystal lattice whereas for $\nu > 0$ the orientation of the vortex lattice is rotated by 45°. Comparing to recent experimental results of Riseman *et al.*[11], who found the vortex and crystal lattices aligned in almost the entire field range, we conclude that $\nu < 0$. The continuous

hex-to-square transition should be observable through Bitter decoration experiments. An alternative signature of this transition is given through the splitting in the peak of the field distribution $P(B)$. These field distributions should be observable in μSR experiments.

Acknowledgments

We thank G. Blatter, E. M. Forgan, G. Luke, A. Mackenzie, Y. Maeno, T. M. Rice, and especially M. Sigrist for helpful discussions. We gratefully acknowledge support by the Swiss Nationalfonds and D. F. A. further acknowledges support from the Natural Science and Engineering Research Council of Canada.

REFERENCES

[1] Y. Maeno, H. Hashimoto, K. Yoshida. S. Nishizaki, T. Fujita, J. G. Bednorz, and F. Lichtenberg, Nature **372**, 532 (1994).

[2] M. Sigrist and K. Ueda, Rev. Mod. Phys. **63**, 239 (1991).

[3] T. Balian and N. R. Werthamer, Phys. Rev. **131**, 1553 (1963).

[4] T. M. Rice and M. Sigrist, J. Phys. Condens. Matter **7**, L643 (1995).

[5] G. M. Luke, Y. Fudamoto, K. M. Kojima, M. I. Larkin, J. Merrin, B. Nachumi, Y. J. Uemura, Y. Maeno, Z. Q. Mao, Y. Mori, H. Nakamura, and M. Sigrist, Nature (London) **394**, 558 (1998).

[6] D. F. Agterberg, Phys. Rev. Lett. **80**, 5184 (1998).

[7] A. P. Mackenzie, S. R. Julian, A. J. Diver, G. G. Lonzarich, Y. Maeno, S. Nishizaki, and T. Fujita, Phys. Rev. Lett. **76**, 3786 (1996).

[8] T. Oguchi, Phys. Rev. B **51**, 1385 (1995).

[9] D. J. Singh, Phys. Rev. B **52**, 1358 (1995).

[10] D. F. Agterberg, T. M. Rice, and M. Sigrist, Phys. Rev. Lett. **78**, 3374 (1997).

[11] T. M. Riseman, P. G. Kealy, E. M. Forgan, A. P. Mackenzie, L. M. Galvin, A. W. Tyler, S. L. Lee, C. Ager, D. McK. Paul, C. M. Aegerter, R. Cubitt, Z. Q. Mao, S. Akima, and Y. Maeno, Nature (London), in press.

[12] T. Imai, A. W. Hunt, K. R. Thurber, and F. C. Chou, Phys. Rev. Lett. **81**, 3006 (1998).

[13] V. G. Kogan, A. Gurevich, J. H. Cho, D. C. Johnston, Ming Xu, J. R. Thompson, and A. Martynovich, Phys. Rev. B **54**, 12386 (1996).

[14] K. Park and D. A. Huse, Phys. Rev. B **58**, 9427 (1998).

[15] I. Affleck, M. Franz, and M. H. S. Amin, Phys. Rev. B **55**, R704 (1997).

[16] Y. De Wilde, M. Iavarone, U. Welp, V. Metlushko, A. E. Koshelev, I. Aranson, G. W. Crabtree, and P. C. Canfield, Phys. Rev. Lett. **78**, 4273 (1997).

[17] A. P. Mackenzie, R. K. W. Haselwimmer, A. W. Tyler, G. G. Lonzarich, Y. Mori, S. Nishizaki, and Y. Maeno, Phys. Rev. Lett. **80**, 161 (1998).

[18] D. F. Agterberg, Phys. Rev. B, to appear Dec. 1, 1998.

[19] R. Heeb, A. van Otterlo, M. Sigrist, and G. Blatter, Phys. Rev. B **54**, 9385 (1996).

[20] P. I. Soininen, C. Kallin, and A. J. Berlinsky, Phys. Rev. B **50**, 13883 (1994).

[21] A. J. Berlinsky, A. L. Fetter, M. Franz, C. Kallin, and P. I. Soininen, Phys. Rev. Lett. **75**, 2200 (1995).

[22] M. Franz, C. Kallin, P. I. Soininen, A. J. Berlinsky, and A. L. Fetter, Phys. Rev. B **53**, 5795 (1996).

[23] M. Ichioka, N. Hayashi, N. Enomoto, and K. Machida, Phys. Rev. B **53**, 2233 (1996).

[24] E. H. Brandt, J. Low Temp. Phys. **26**, 709, 735 (1977).

FIGURES

FIG. 1. Exponent Λ governing the decay of $\nu = 0$ solutions.

FIG. 2. Contour plot of GL-calculations for the absolute values of the dominant η_-- (a) and the admixed η_+-component (b) for the parameters $\kappa = 2.5$ and $\nu = -0.3$. The contours are 0.99, 0.975, ... for (a) and 0.03, 0.045, ..., 0.225 for (b)

FIG. 3. Contour plot of the absolute value of the $|B|$-field for the same parameters as in Fig. 2. Notice the strong square deformations of the vortex core along the diagonals of the crystal lattice. The contours are 0.03, 0.06, ..., 0.42.

FIG. 4. Schematic illustration of the real unit cell.

FIG. 5. Vortex lattice structure as function of the applied field H. The GL-parameter is $\kappa = 2.5$ (a) and $\kappa = 25.0$ (b), and θ_2 denotes the angle between the unit cell vectors minimizing the free energy density given in Eq. (24).

FIG. 6. Contour plot of the field distribution for $\nu = -0.4, \kappa = 2.5, H = 0.25$. The horizontal and vertical axes of the plot correspond to the axes of the underlying crystal lattice. The field distribution shows an aligned square lattice with weak square shaped deformations of the vortex cores.

FIG. 7. Field distribution $P(B)$ for different values of the anisotropy ν at $\kappa = 2.5, H = 0.3$ (a) and $\kappa = 25.0, H = 3.1$ (b).

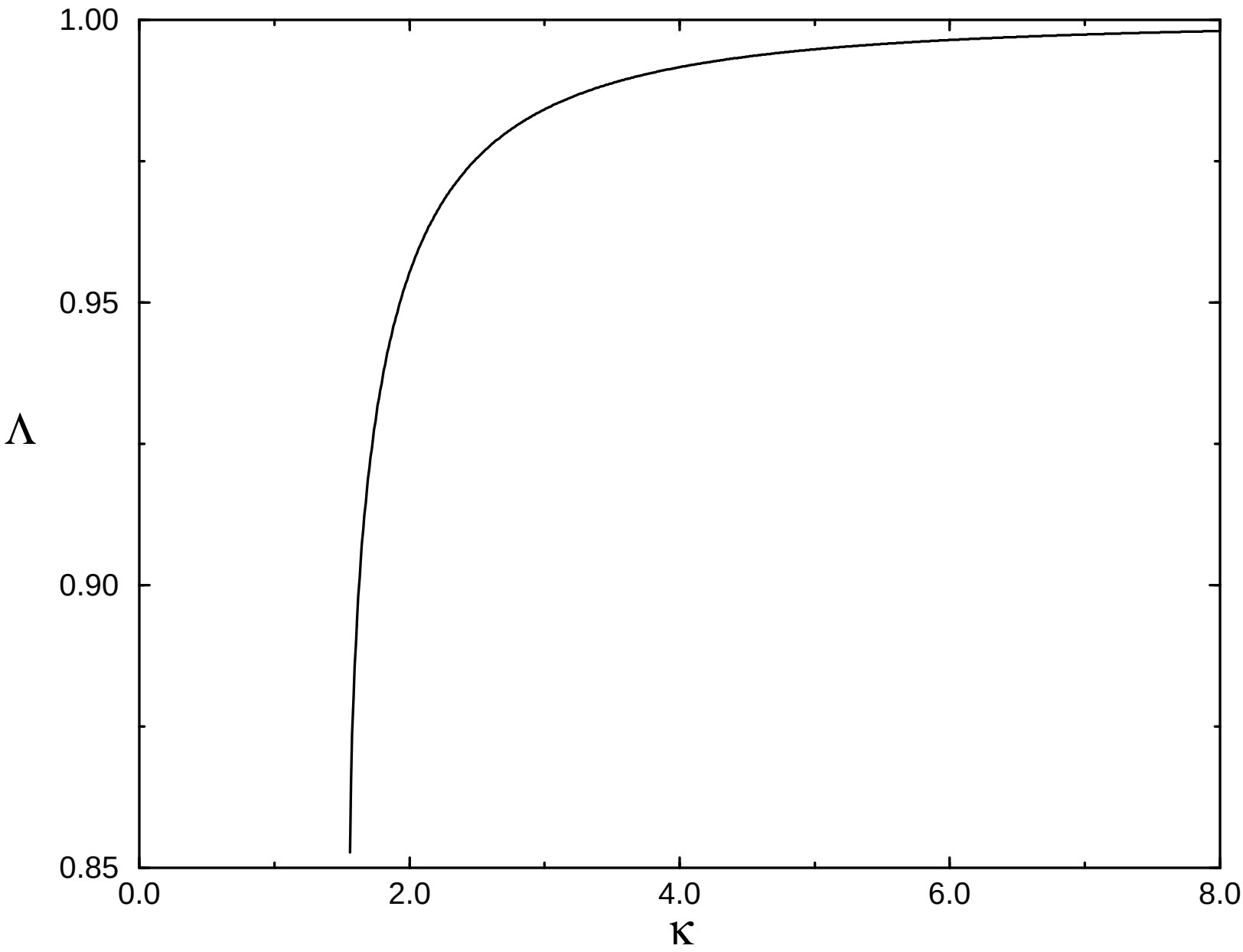
1.00
0.95
0.90
0.85
Λ
0.0
2.0
4.0
6.0
8.0
κ

a

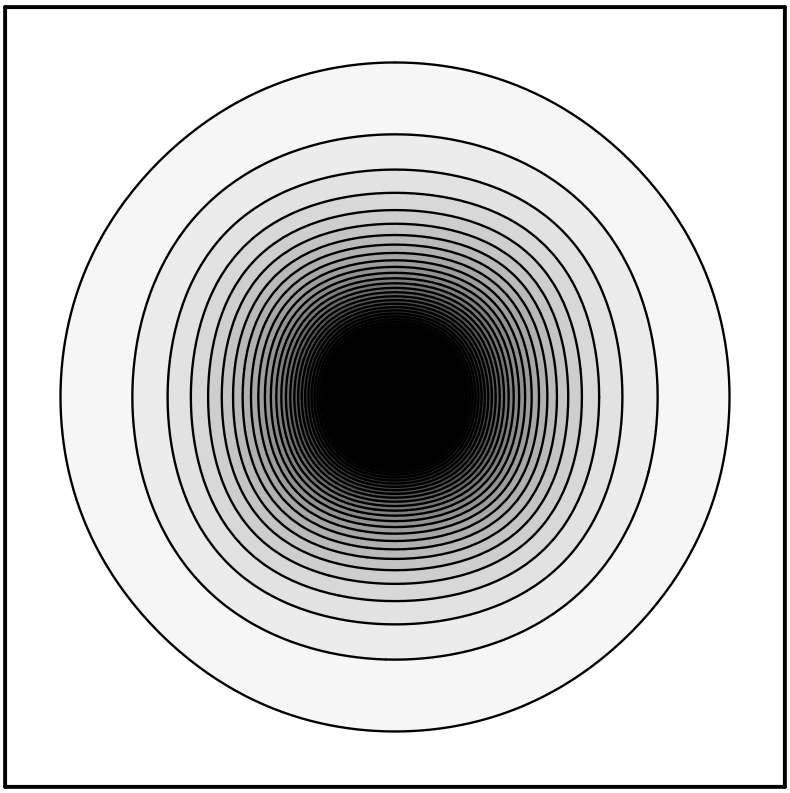

b

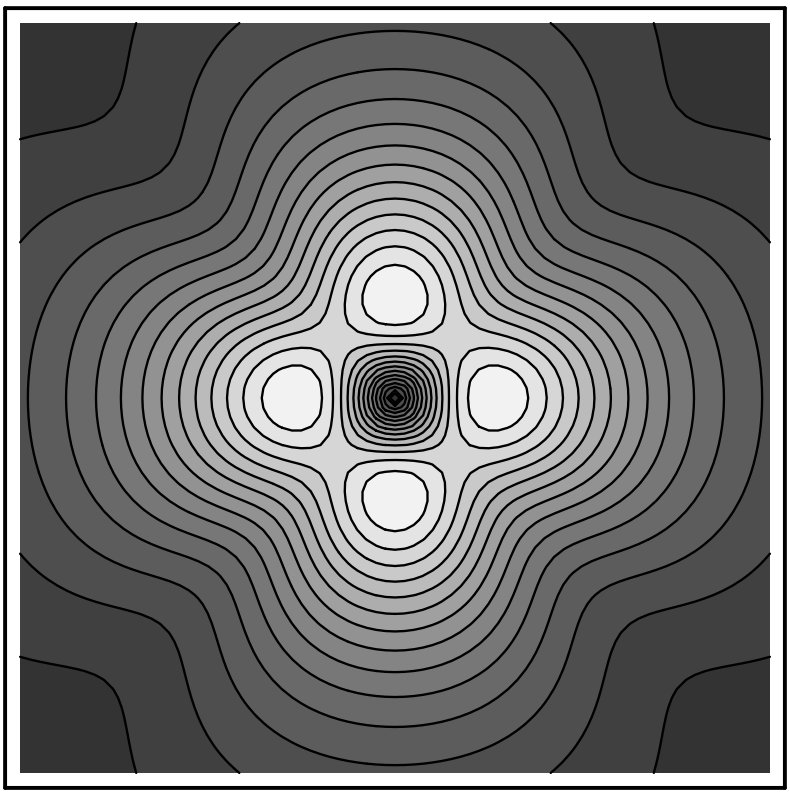

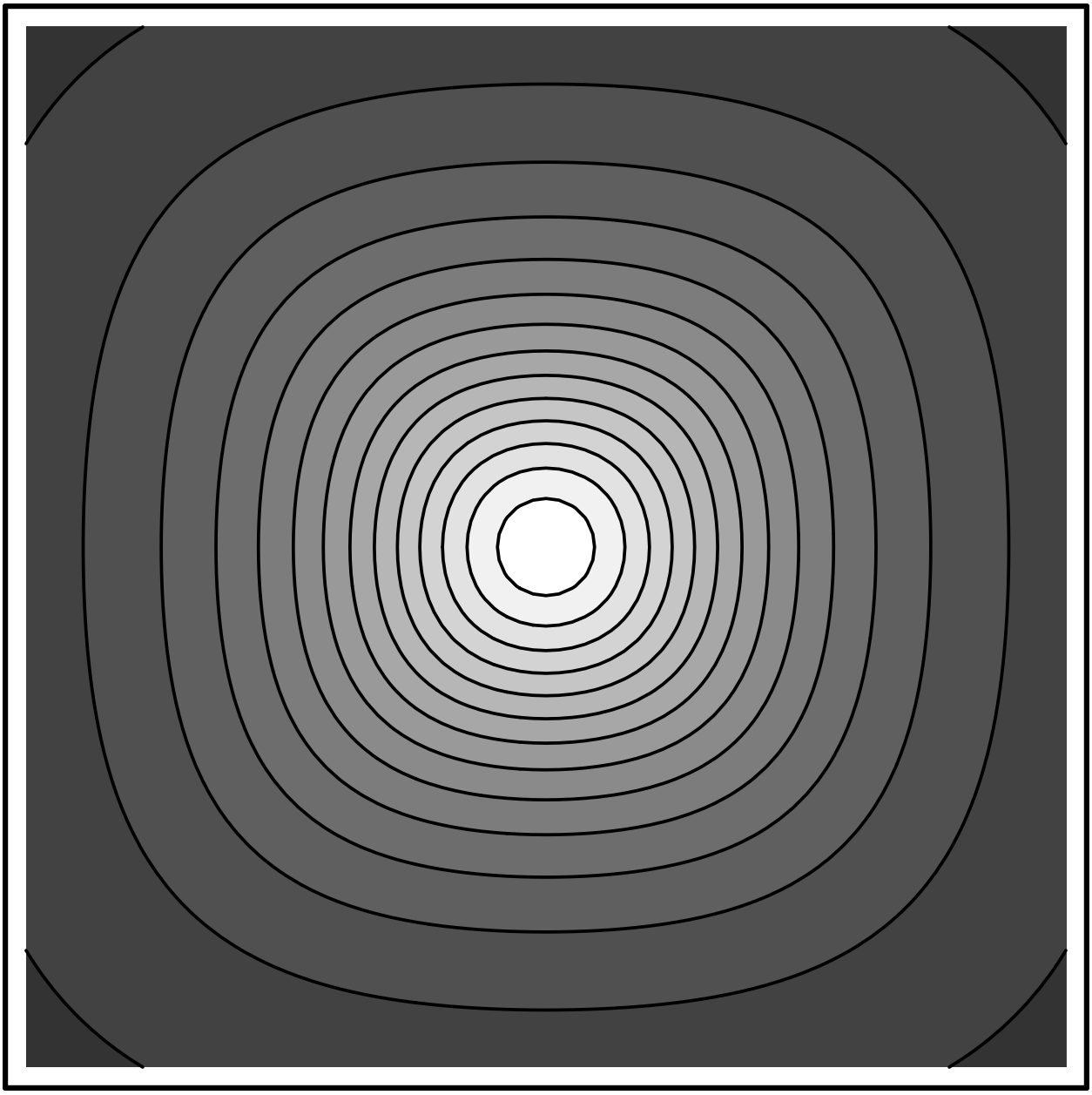

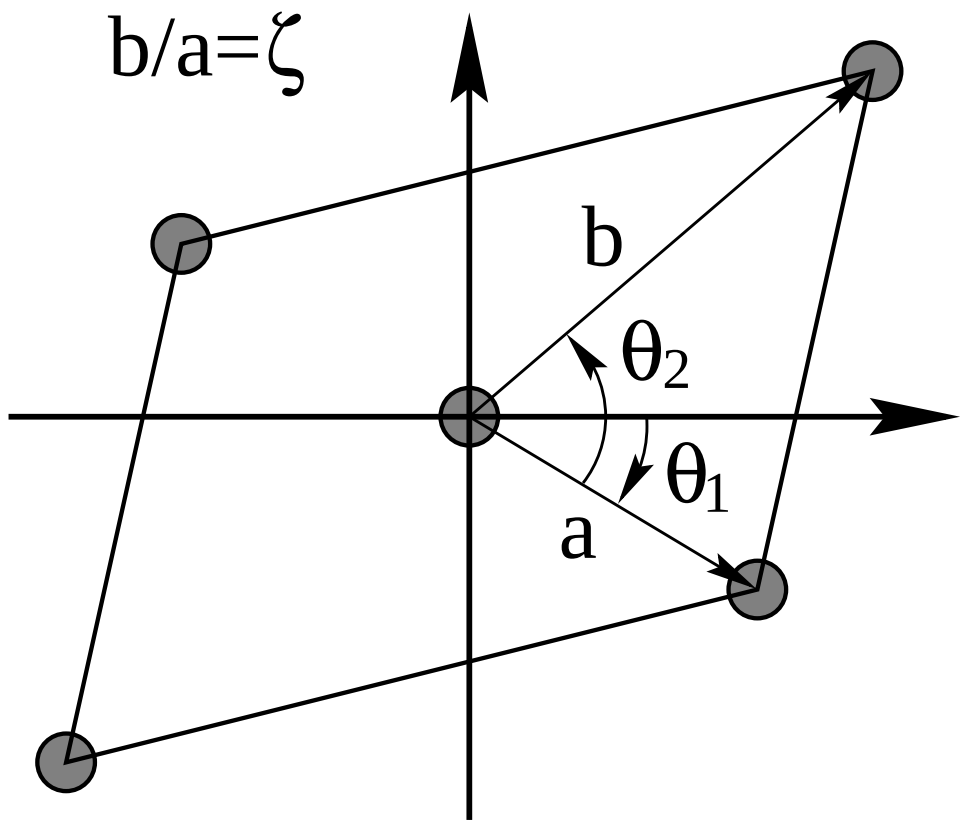
b/a=ζ
b
θ2
θ1
a

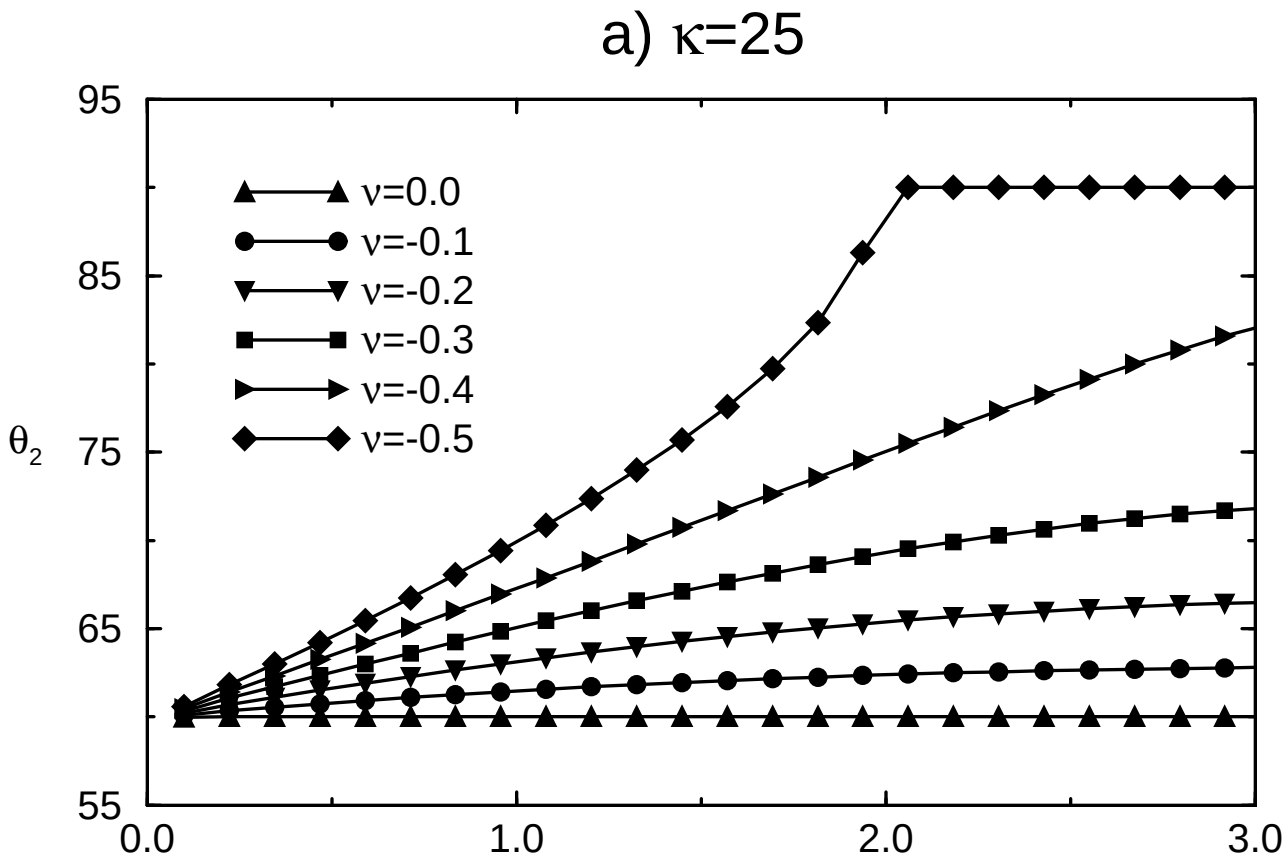
a) κ=25
95
85
75
65
55
θ2
0.0
1.0
2.0
3.0
ν=0.0
ν=-0.1
ν=-0.2
ν=-0.3
ν=-0.4
ν=-0.5

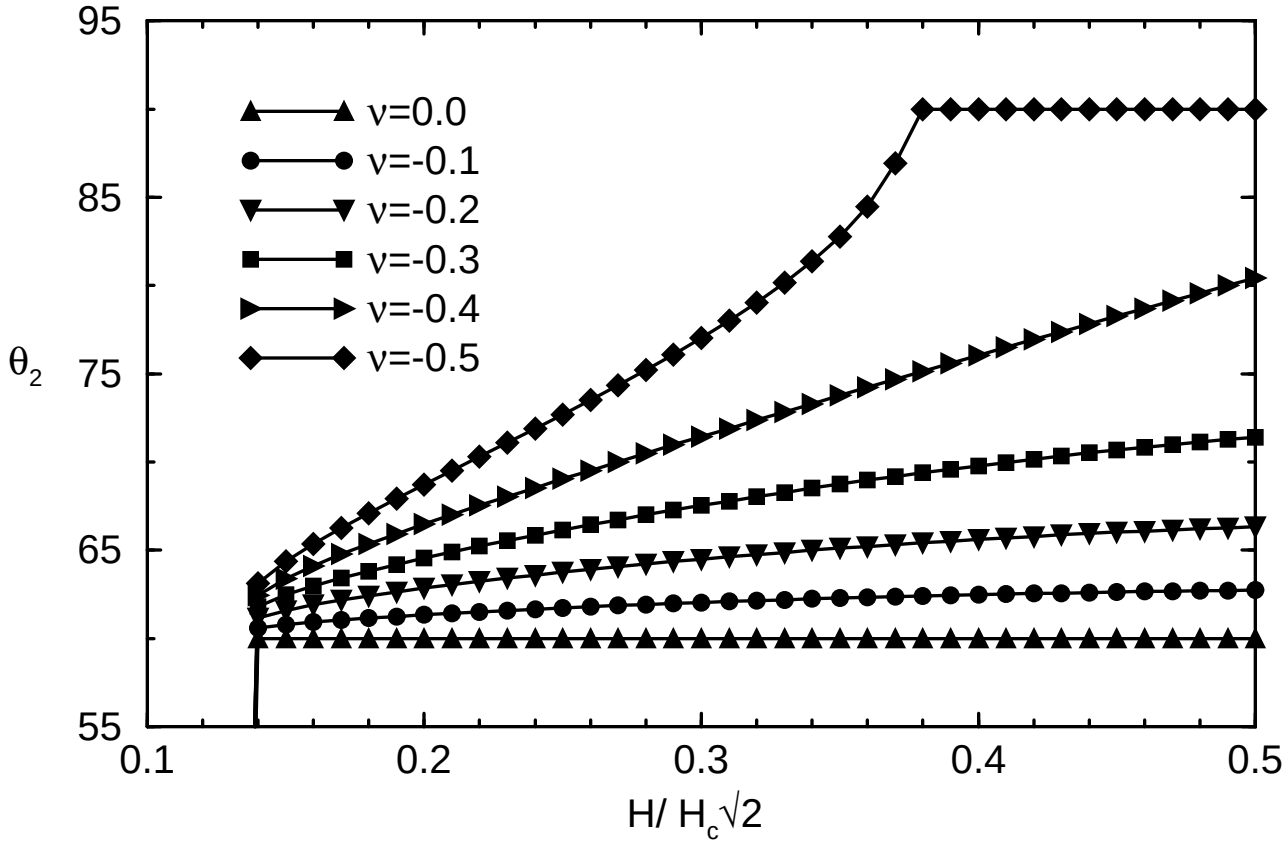
b) κ=5.0
95
85
75
65
55
θ2
0.1
0.2
0.3
0.4
0.5
H/ Hc√2
ν=0.0
ν=-0.1
ν=-0.2
ν=-0.3
ν=-0.4
ν=-0.5

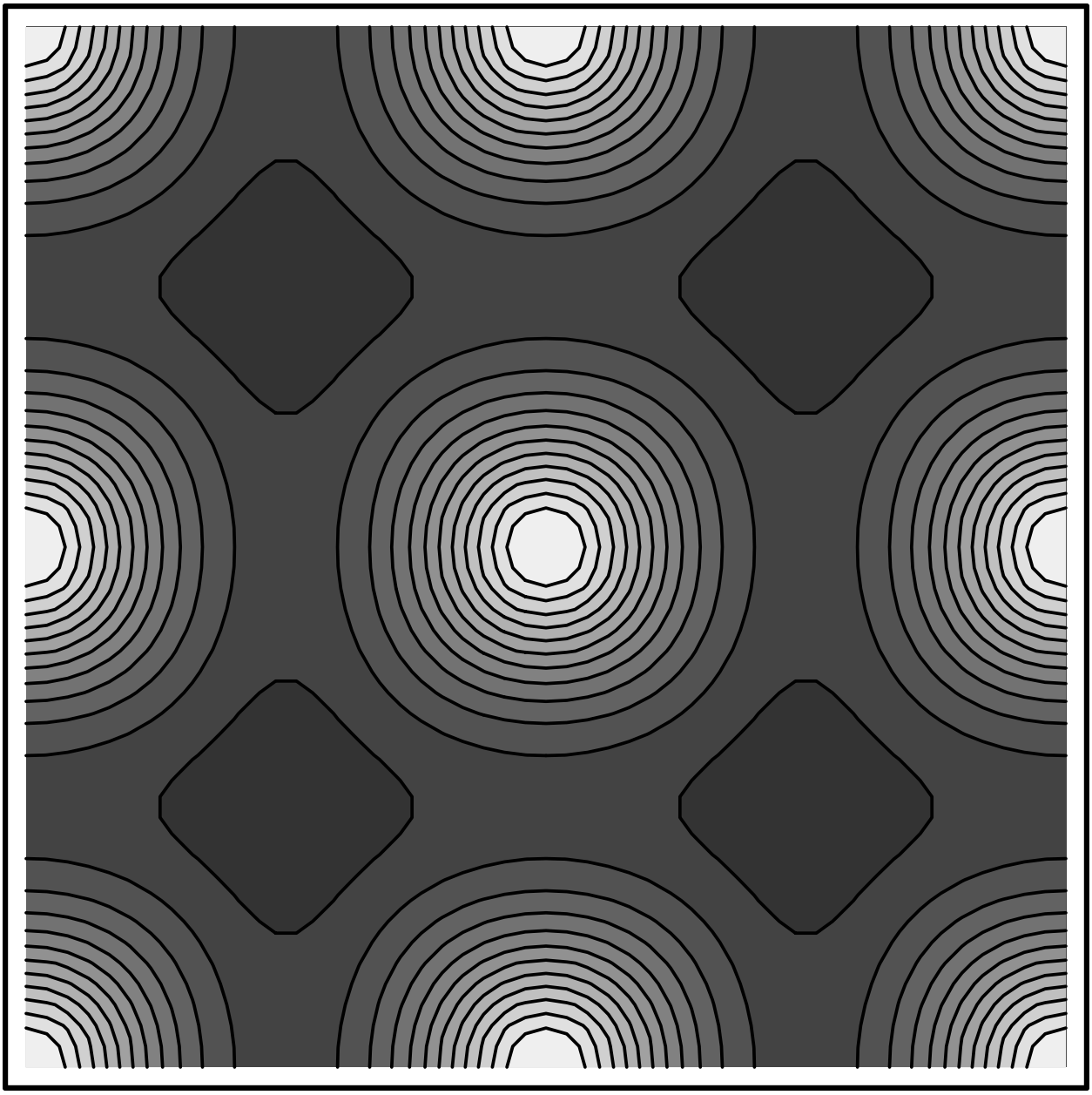

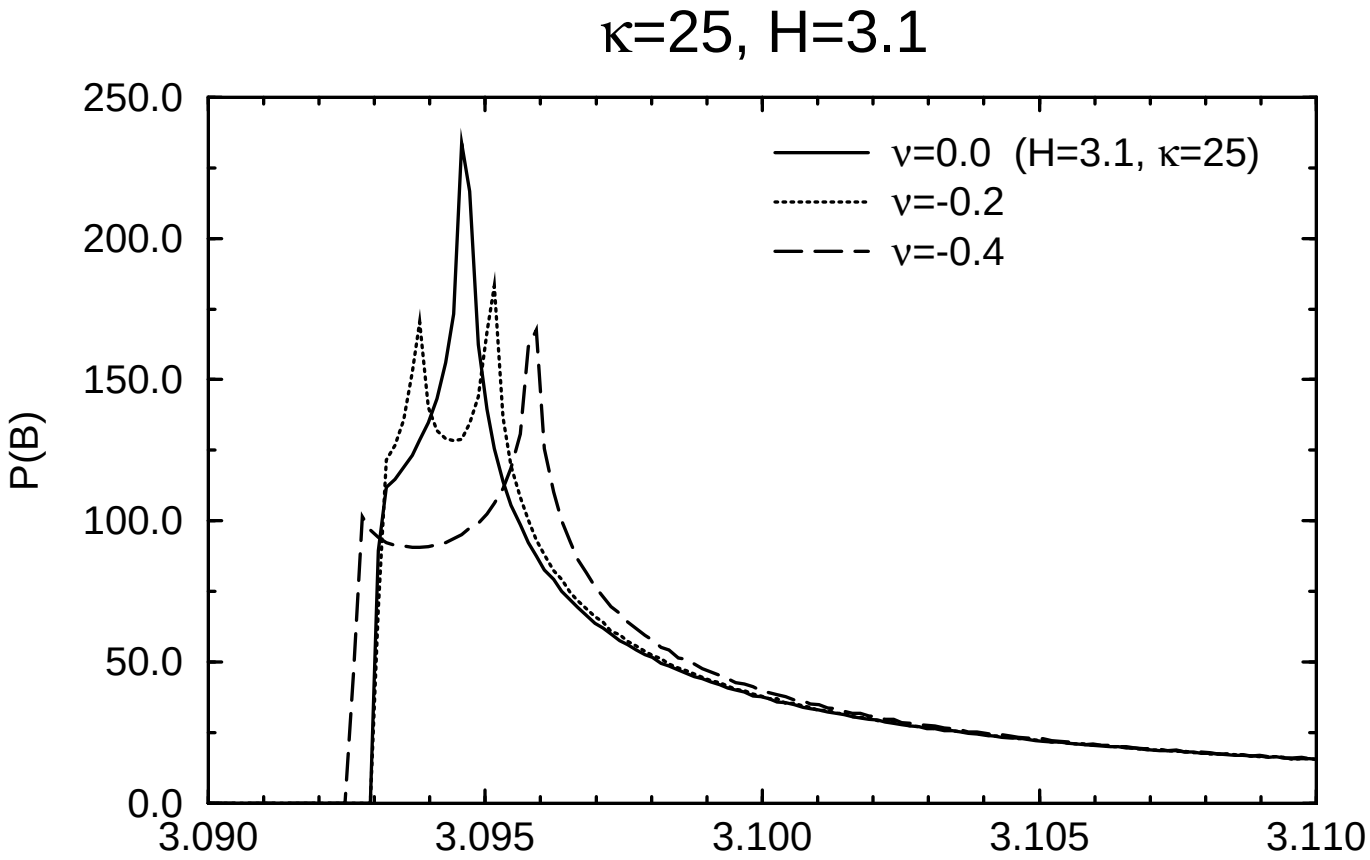
κ=25, H=3.1
P(B)
250.0
200.0
150.0
100.0
50.0
0.0
3.090
3.095
3.100
3.105
3.110
ν=0.0 (H=3.1, κ=25)
ν=-0.2
ν=-0.4

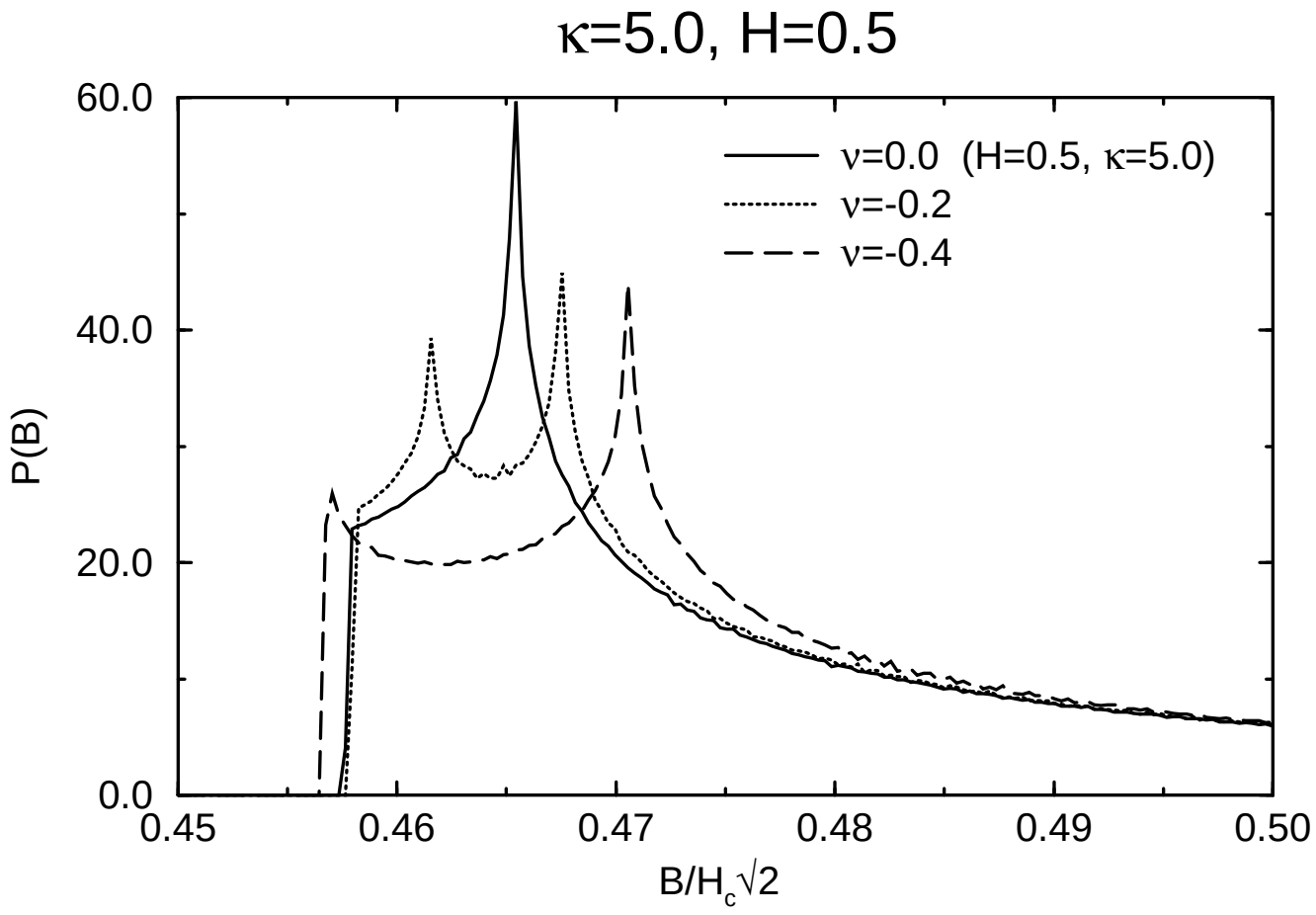
κ=5.0, H=0.5
P(B)
60.0
40.0
20.0
0.0
0.45
0.46
0.47
0.48
0.49
0.50
B/H_c√2
ν=0.0 (H=0.5, κ=5.0)
ν=-0.2
ν=-0.4